INTERNATIONAL JOURNAL OF
NUMERICAL ANALYSIS AND MODELING
Volume 14, Number 6, Pages 879–892

A NOVEL ADAPTIVE FINITE VOLUME METHOD FOR ELLIPTIC EQUATIONS

YANHUI ZHOU AND QINGSONG ZOU

Abstract. In this paper, we propose a novel adaptive finite volume method (AFVM) for elliptic equations. As a standard adaptive method, a loop of our method involves four steps: $Solve \rightarrow Estimate \rightarrow Mark \rightarrow Refine$. The novelty of our method is that we do not have the traditional "completion" procedure in the *Refine* step. To guarantee the conformity, a triangular element with a hanging node is treated as a quadrilateral element, and the corresponding function space consists of the bilinear functions. The optimal computational complexity of our AFVM is validated by numerical examples.

Key words. Adaptive finite volume method, hanging nodes, hybrid meshes, error analysis.

1. Introduction

The finite volume method (FVM) is a popular numerical tool for partial differential equations (PDEs), cf. [1, 2, 5, 13–18, 20–22, 24–26, 28, 29, 31–33, 37]. Recently, the adaptive finite volume method (AFVM) attracts a lot of attention, see [6,8,11,12,19,23,27,30,36]. Especially the a *posteriori* error estimator has been studied in many papers, see [36] for the hierarchical type and [6, 11, 12, 23, 27, 30] the residual type error estimators.

In this paper, we design a novel AFVM for elliptic equations. Unlike the previous works which pay a lot of attention on the construction of a *posteriori* error estimators for the FVM, here we construct our novel adaptive method modifying the adaptive strategy. It is known that an iteration of a standard adaptive method involves four steps: $Solve \rightarrow Estimate \rightarrow Mark \rightarrow Refine$. In particular, in the *Refine* step, after having refined the mesh according to the previous marking step, we should refine more elements to eliminate the so called "hanging nodes". The novelty of our method is that we do not have the traditional "completion" procedure in the *Refine* step which allow hanging nodes. In order to guarantee the conformity, a triangular element with one hanging node will not be divided if the edge with the hanging node is not a base of the triangle. We consider this triangle with the hanging node as a quadrilateral. We only divide a triangular element has a hanging node on the base, or has more than one hanging nodes on edges. As a consequence, our meshes in AFVM consist of hybrid triangular and quadrilateral elements, to ensure the continuity of our trial function of the finite volume scheme in the *Solve* step, we let the trial function on triangular element be constructed as the linear function and on quadrilateral element (a triangular element with a hanging node) as the isoparametric bilinear. In other words, we define the trial function as

$$\begin{cases} \text{linear function}, & \text{if a triangular element has no hanging node} \\ \text{isoparametric bilinear function}, & \text{if a triangular element has a hanging node} \end{cases}.$$

We follow the Zienkiewicz-Zhu [34, 35] type gradient recovery operator in the *Estimate* step, and the marking strategy proposed by Dörfler [10] in the *Mark* step.

Received by the editors March 5, 2017 and, in revised form, June 2, 2017.
2000 *Mathematics Subject Classification.* 35R35, 49J40, 60G40.

One may naturally ask a question: how about the actual significance of the novel AVFM? It is known that to keep the conformity, in the *Refine* step, one often needs an additive "completion" procedure [3] to eliminate the hanging nodes. Our numerical experiments show that the novel AFVM decrease the steps of bisection for the conformity compare to the standard AFVM which needs traditional "completion" procedure. Moreover, our AFVM possesses the local conservation property. Furthermore, suppose u is the exact solution of the elliptic equation, our numerical results show that

$$|u - u_k|_1 \leq C_1 N_k^{-1/2} \text{ and } \|u - u_k\|_0 \leq C_2 N_k^{-1},$$

where u_k and N_k are the FVM solution and the number of elements of the mesh to k-th iteration, C_1 and C_2 are two constants. We note that in our numerical example, the optimal convergence order of H^1 and L^2 errors can be obtained even if $u \in H^{1+\frac{2}{3}-\varepsilon}(\Omega)$ for all $\varepsilon > 0$ and $u \notin H^2(\Omega)$, and the domain Ω is not convex.

The main idea of our AFVM can be applied to general elliptic equations. To illustrate the basic idea, we focus on the model problem

$$-\nabla \cdot (\alpha \nabla u) = f \quad \text{in } \Omega, \tag{1}$$

$$u = 0 \quad \text{on } \partial\Omega, \tag{2}$$

where $\Omega \subset \mathbb{R}^2$ is a convex polygon domain, α is a piecewise continuous function that bounded below: There exists a positive constant $\alpha_0 > 0$ such that $\alpha(x) \geq \alpha_0$ for almost all $x \in \Omega$, and f is a real valued function defined on Ω. The stability analysis of our finite volume scheme is a routine under the framework of linear on triangular element [29] and isoparametric bilinear on quadrilateral element [25], and we obtain the optimal convergence rate of H^1 and L^2 norms.

The rest of this paper is organized as follows. In the next section we introduce a FVM on hybrid triangular and quadrilateral meshes. The optimal convergence properties are studied both in H^1 and L^2 spaces. Our novel AFVM is presented in Section 3. Numerical examples are provided in Section 4 to validate that our novel AFVM has optimal computational cost and the theoretical results of our FVM.

We end this section with some notations. For an integer $m \geq 0$ and $1 \leq p \leq \infty$, $W^{m,p}(\Omega)$ denote the standard Sobolev spaces of functions that have generalized derivatives up to order m in $L^p(\Omega)$. The norm (or semi-norm) is defined by $\|u\|_{m,p,\Omega} = \left(\sum_{|\alpha|\leq m} \|D^\alpha u\|_p^p\right)^{1/p}$ (or $|u|_{m,p,\Omega} = \left(\sum_{|\alpha|=m} \|D^\alpha u\|_p^p\right)^{1/p}$) for $1 \leq p < \infty$, and with the standard modification for $p = \infty$. $H^m(\Omega) := W^{m,2}(\Omega)$ and $H_0^1(\Omega)$ denote the subspace of $H^1(\Omega)$ of functions vanishing on the boundary $\partial\Omega$. For simplicity, in the rest of the paper we will omit the subscript index when $p = 2$ and the domain index Ω if needed. Furthermore, $(\cdot, \cdot)$ denotes the standard $L^2(\Omega)$-inner product. To avoid writing constants repeatedly, "$A \lesssim B$" means that A can be bounded by B multiplied by a constant which is independent of the parameters which A and B may depend on, "$A \gtrsim B$" means that B can be bounded by A. "$A \sim B$" means "$A \lesssim B$" and "$B \lesssim A$".

2. A finite volume method on hybrid meshes

2.1. A hybrid triangular and quadrilateral mesh. We partition Ω into a mesh $\mathcal{T}_h$ consisting of a finite number of triangles and convex quadrilaterals, where h is the largest diameter of all triangles and quadrilaterals, and we call $\mathcal{T}_h$ the primal mesh of Ω, see Fig.1. We denote by $\mathcal{N}_h$ the set of all vertices of $\mathcal{T}_h$, and let $\mathcal{N}_h^\circ = \mathcal{N}_h \backslash \partial\Omega$ be the set of all interior vertices.

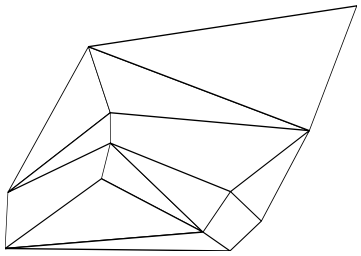

FIGURE 1. A hybrid triangular and quadrilateral mesh.

Suppose $P_i(i = 1, 2, 3, 4)$ are four vertices of quadrilateral $\tau_Q \in \mathcal{T}_h$, M_i is the midpoint of the edge $\overline{P_iP_{i+1}}$ $(i = 1, 2, 3, 4)$. We denote Q as the intersection point of $\overline{M_1M_3}$ and $\overline{M_2M_4}$, and call point Q as the averaging center of τ_Q. We denote S_Q and d_Q as the area of τ_Q and the length $|\overrightarrow{P_1P_2} + \overrightarrow{P_3P_4}|$ respectively. We note that the length d_Q equals to the distance vector of the diagonal midpoints of τ_Q. Moreover, if τ_Q is a parallelogram, then $d_Q = 0$.

We call a partition $\mathcal{T}_h$ *conform* if different triangles and quadrilaterals in $\mathcal{T}_h$ have no common interior points, and a vertex of any triangle or quadrilateral does not lie on the interior of an edge of any other triangle or quadrilateral.

A partition $\mathcal{T}_h$ is called *shape regular* provided the following conditions are satisfied:

(i) For each triangle $\tau_T \in \mathcal{T}_h$, there exists a positive constant c_1 independent of h such that $\frac{h_T}{\rho_T} \leq c_1$, where h_T is the largest diameter of τ_T and ρ_T is the maximum diameter of circles contained in τ_T.

(ii) For each quadrilateral $\tau_Q \in \mathcal{T}_h$, the ratio of the maximal edge to minimal edge lengths is bounded by a constant, and the four angles are bigger than θ_0 and smaller than $\pi - \theta_0$ with some $\theta_0 > 0$.

We call a partition $\mathcal{T}_h$ *quasi uniform* if $\mathcal{T}_h$ is shape regular and satisfies the following conditions:

(i) For each triangle $\tau_T \in \mathcal{T}_h$, there exists a positive constant c_2 independent of h such that $\frac{h}{\rho_T} \leq c_2$.

(ii) For each quadrilateral $\tau_Q \in \mathcal{T}_h$, $S_Q \sim h^2$, $d_Q \lesssim h^2$.

2.2. A finite volume scheme on hybrid meshes. Our finite volume scheme is based on the framework of Petrov-Galerkin method. We first construct the trial function space. For any quadrilateral $\tau_Q \in \mathcal{T}_h$, there exists a unique invertible bilinear transformation F_{τ_Q} maps the reference unit square $\widehat{\tau}_Q = [0, 1]^2$ to τ_Q (cf. [4]). With respect to $\mathcal{T}_h$, we define the trial function space

$$U_h = \{v_h \in C(\overline{\Omega}) : \begin{array}{ll} v_h|_{\tau_T} \in \mathcal{P}_1, & \forall \tau_T \in \mathcal{T}_h \\ v_h|_{\tau_Q} \in \mathcal{Q}_1(\widehat{\tau}_Q) \circ F_{\tau_Q}^{-1}, & \forall \tau_Q \in \mathcal{T}_h \end{array} ; v_h|_{\partial\Omega} = 0\}, \tag{3}$$

where $\mathcal{P}_1$ and $\mathcal{Q}_1$ are the sets of all polynomials and bi-polynomials of degree no more than 1 respectively, τ_T and τ_Q are the triangular and quadrilateral element of $\mathcal{T}_h$, $F_{\tau_Q}^{-1}$ denotes the inverse of the transformation F_{τ_Q}, and $\mathcal{Q}_1(\widehat{\tau}_Q) \circ F_{\tau_Q}^{-1}$ is a composite function. From the definition of U_h, we have

$$\dim U_h = \#\mathcal{N}_h^0, \tag{4}$$

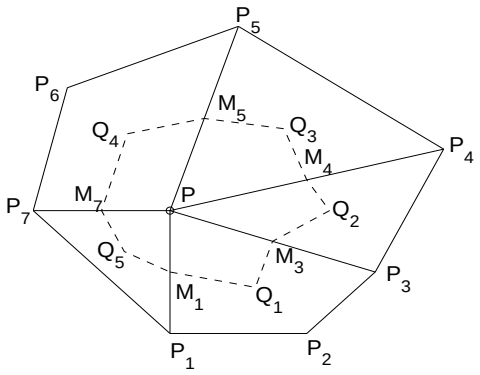

FIGURE 2. A control volume V_P associated with a node P of a hybrid mesh.

where $\dim S$ and $\#S$ are the dimension and cardinality of the set S.

Now, we proceed to present the dual partition of Ω and the corresponding test function space. The dual partition is another mesh of Ω, and the test function space is based on the dual mesh. The dual partition of Ω is constructed as follows. For each vertex P of $\mathcal{T}_h$ (see Fig.2), the point P is a common vertex of $\square PP_1P_2P_3$, $\triangle PP_3P_4$, $\triangle PP_4P_5$, $\square PP_5P_6P_7$, $\triangle PP_7P_1$. Let Q_1, Q_4 be the averaging centers of $\square PP_1P_2P_3$, $\square PP_5P_6P_7$; and Q_2, Q_3, Q_5 be the barycenters of $\triangle PP_3P_4$, $\triangle PP_4P_5$, $\triangle PP_7P_1$; and M_1, M_3, M_4, M_5, M_7 be the midpoints of edges $\overline{PP_1}, \overline{PP_3}, \overline{PP_4}, \overline{PP_5}, \overline{PP_7}$. Then we connect points $M_1, Q_1, M_3, Q_2, M_4, Q_3, M_5, Q_4$, M_7, Q_5, M_1 successively to obtain a polygonal domain V_P surrounding point P, and call V_P a control volume with respect to the vertex P. Let $\mathcal{T}_h'$ be a dual partition of Ω if $\mathcal{T}_h'$ is constructed by all control volumes V_P, $P \in \mathcal{N}_h$. In other words, we define

$$\mathcal{T}_h' = \{V_P : P \in \mathcal{N}_h\}.$$

The corresponding test function space V_h contains all the piecewise constant functions with respect to $\mathcal{T}_h'$ defined as

$$V_h = \mathrm{Span}\{\psi_{V_P} : P \in \mathcal{N}_h^0\},$$

where ψ_{V_P} is the characteristic function on V_P. Similar to (4), we have

$$\dim V_h = \#\mathcal{N}_h^0. \tag{5}$$

It follows from (4) and (5) that

$$\dim U_h = \dim V_h = \#\mathcal{N}_h^0. \tag{6}$$

We are now ready to describe the finite volume scheme on hybrid meshes. The finite volume solution of Eqs. (1) and (2) is a function $u_h \in U_h$ which satisfies the following conservation law

$$-\int_{\partial V_P} \alpha \frac{\partial u_h}{\partial \mathbf{n}}\,\mathrm{d}s = \int_{V_P} f\,\mathrm{d}x\mathrm{d}y \tag{7}$$

on each control volume V_P, $P \in \mathcal{N}_h^0$, where $\mathbf{n}$ is the unit outward normal on the boundary ∂V_P. Let $w_h \in V_h$, and w_h can be written as

$$w_h = \sum_{P \in \mathcal{N}_h^0} w_P \psi_{V_P},$$

where the coefficients w_P, $P \in \mathcal{N}_h^0$ of w_h are constants. Multiplying (7) with w_P and then summing up for all $P \in \mathcal{N}_h^0$, then we obtain

$$-\sum_{P\in\mathcal{N}_h^0} w_P \int_{\partial V_P} \alpha \frac{\partial u_h}{\partial \mathbf{n}}\,\mathrm{d}s = \int_\Omega f w_h\,\mathrm{d}x\mathrm{d}y.$$

Define the finite volume scheme bilinear form for all $v \in H_0^1(\Omega)$, $w_h \in V_h$ as

$$a_h(v, w_h) = -\sum_{P\in\mathcal{N}_h^0} w_P \int_{\partial V_P} \alpha \frac{\partial u_h}{\partial \mathbf{n}}\,\mathrm{d}s.$$

The finite volume scheme for solving Eqs. (1) and (2) reads as: Find $u_h \in U_h$ such that

$$a_h(u_h, w_h) = (f, w_h),\ \forall w_h \in V_h. \tag{8}$$

2.3. Stability and convergence. From (6) we define a linear bijective mapping $\Pi_h : v_h \in U_h \to V_h$ such that

$$\Pi_h v_h(P) = v_h(P),\ \forall P \in \mathcal{N}_h.$$

Theorem 2.1. *Suppose $\mathcal{T}_h$ is a conform and shape regular hybrid mesh, and the coefficient α is a piecewise constant with respect to $\mathcal{T}_h$, then*

$$a_h(v_h, \Pi v_h) \gtrsim |v_h|_{1,\Omega}^2,\ \forall v_h \in U_h. \tag{9}$$

Consequently, Let $u \in H_0^1(\Omega) \cap H^2(\Omega)$ be the exact solution of (1) *and* (2)*, $u_h \in U_h$ be the numerical solution of* (8)*. We have*

$$|u - u_h|_1 \lesssim h|u|_2. \tag{10}$$

Furthermore, if $\mathcal{T}_h$ is a quasi uniform hybrid mesh and $f \in H^1(\Omega)$, $\alpha \in W^{2,\infty}(\Omega)$, then

$$\|u - u_h\|_0 \lesssim h^2\|f\|_1. \tag{11}$$

Proof. We have the coercivity of triangular [29] and quadrilateral [25] meshes respectively, then summing up them we obtain (9). The H^1 error estimate (10) is a routine by (9). Similar to the L^2 error estimate on triangular [13] and quadrilateral [21] meshes, (11) can be proved by Aubin-Nitsche technique [4, 9]. □

Remark 2.1. In the Section 4, numerical example 4.1 shows that we also obtained the optimal convergence rate of L^2 norm even if $\mathcal{T}_h$ is not quasi uniform; examples 4.2 and 4.3 show that the above FVM is stable even if $\mathcal{T}_h$ is not shape regular.

Now, we are ready to introduce a novel hybrid mesh. In Fig.3, there are three triangles $\triangle P_1P_2P_4$, $\triangle PP_2P_3$ and $\triangle PP_3P_4$, it is a triangular mesh. However, this mesh can not ensure the conformity since there exists a hanging node P. To guarantee the conformity, we consider this triangular grid as a novel hybrid mesh when we treat $\triangle P_1P_2P_4$ with the hanging node P as a quadrilateral $P_4P_1P_2P$. This new feature is great useful to the following adaptive finite volume method since it allow hanging nodes.

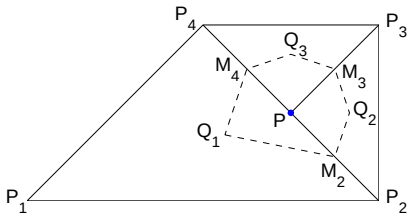

FIGURE 3. Treat $\triangle P_1P_2P_4$ with the hanging node P as a quadrilateral and the control volume V_P.

3. A novel adaptive finite volume method

In this section, we present a novel adaptive finite volume method (AFVM) for (1) and (2). Our AFVM is a loop involves: $Solve \rightarrow Estimate \rightarrow Mark \rightarrow Refine$. The novelty of our method is that we do not have the traditional "completion" procedure in the *Refine* step. Let $\mathcal{T}_k$ be the k-th iteration mesh of Ω, and suppose $\mathcal{T}_1$ is a triangular mesh. For convenience, we denote $u_k := u_{\mathcal{T}_k}$, $\eta_k(u_k,\tau)_{\tau\in\mathcal{T}_k} := \eta_{\mathcal{T}_k}(u_{\mathcal{T}_k},\tau)_{\tau\in\mathcal{T}_k}$, $\mathcal{M}_k := \mathcal{M}_{\mathcal{T}_k}$, and N_k as the number of elements of the mesh $\mathcal{T}_k$.

Firstly, we discuss the *Solve* subroutine. For the mesh $\mathcal{T}_k$, the subroutine

$$u_k = Solve(\mathcal{T}_k)$$

outputs the finite volume solution u_k of (1) and (2). We note that $\mathcal{T}_k$ ($k \geq 2$) may be hybrid triangular and quadrilateral meshes, since in the $Refine$ step there produce quadrilateral element (a triangular element with a hanging node). Therefore, the trial function space of mesh $\mathcal{T}_k$ ($k \geq 2$) should be linear function on triangular element and bilinear on quadrilateral, which is different from $\mathcal{T}_1$. For example, in Fig.3, it should be linear on triangular elements $\triangle PP_2P_3$ and $\triangle PP_3P_4$, and bilinear on quadrilateral $P_4P_1P_2P$. Moreover, for the mesh $\mathcal{T}_k$ ($k \geq 2$), the trial function space can be rewritten as

$$U_h = \{v_h \in C(\overline{\Omega}) : \begin{array}{ll} v_h|_\tau \in \mathcal{P}_1, & \text{if } \tau \text{ has no hanging node} \\ v_h|_\tau \in \mathcal{Q}_1(\widehat{\tau}) \circ F_\tau^{-1}, & \text{if } \tau \text{ has a hanging node} \end{array} ; v_h|_{\partial\Omega} = 0\}.$$

Secondly, we present gradient recovery error estimator for the finite volume solution u_k and the corresponding mesh $\mathcal{T}_k$. Define $G : u_k \in U_h \rightarrow Gu_k \in (W_h)^2$ be a Zienkiewicz-Zhu [34, 35] type gradient recovery operator, such that for arbitrary vertex $P \in \mathcal{N}_h$

$$Gu_k(P) = \frac{1}{|w_P|} \iint_{w_P} \nabla u_k \, \mathrm{d}x\mathrm{d}y,$$

where

$$W_h := \{v_h \in C(\overline{\Omega}) : \begin{array}{ll} v_h|_\tau \in \mathcal{P}_1, & \text{if } \tau \text{ has no hanging node,} \\ v_h|_\tau \in \mathcal{Q}_1(\widehat{\tau}) \circ F_\tau^{-1}, & \text{if } \tau \text{ has a hanging node,} \end{array} \forall \tau \in \mathcal{T}_h\},$$

$$w_P := \bigcup \{\tau \in \mathcal{T}_k : P \in \tau\}$$

and $|w_P|$ is the area of w_P. Then the subroutine

$$\eta_k(u_k,\tau)_{\tau\in\mathcal{T}_k} = Estimate(\mathcal{T}_k, u_k)$$

outputs the gradient recovery local indicator defined by

$$\eta_k(u_k,\tau) := \|Gu_k - \nabla u_k\|_{0,\tau}, \ \forall \tau \in \mathcal{T}_k.$$

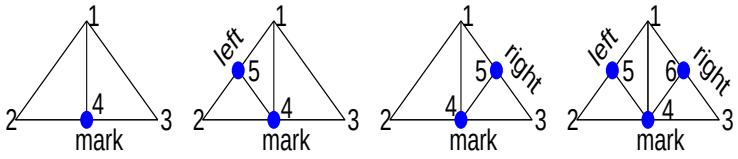

FIGURE 4. Divide a triangle $p(1)p(2)p(3)$ for reducing the error.

Thirdly, we use the marking strategy proposed by Dörfler [10] to mark $\mathcal{T}_k$. For arbitrary subset $\mathcal{S}$ of the mesh $\mathcal{T}_k$, we define

$$\eta_k^2(u_k, \mathcal{S}) := \sum_{\tau \in \mathcal{S}} \eta_k^2(u_k, \tau)$$

as the global error estimator on $\mathcal{S}$. Let the local indicators $\eta_k(u_k, \tau), \tau \in \mathcal{T}_k$ ordered from the largest to the smallest according to their size, then we choose a subset $\mathcal{M}_k \subset \mathcal{T}_k$ with minimal cardinality such that

$$\eta_k^2(u_k, \mathcal{M}_k) \geq \theta \eta_k^2(u_k, \mathcal{T}_k), \tag{12}$$

where $\theta \in (0, 1)$ is a given constant. In short, the subroutine

$$\mathcal{M}_k = Mark(\eta_k(u_k, \tau)_{\tau \in \mathcal{T}_k}, \mathcal{T}_k, \theta)$$

outputs the subset $\mathcal{M}_k$ which satisfies (12).

In the last *Refine* step, we use the longest edge bisection [7]. There are three procedures to accomplish this step. Firstly, marking the subset $\mathcal{M}_k$ for reducing the error. Secondly, marking edges for the conformity. Finally, refining the mesh $\mathcal{T}_k$. We include two parts to interpret them below. The first part illustrate how to implement them in the first loop of our AFVM. The second part describe the difference between the first and remainder loops of AFVM in the *Refine* step.

For each triangular element $\tau \in \mathcal{T}_1$, we label the longest edge of τ as *base* or *refinement edge*. The opposite vertex of the base is called *peak*. Firstly, for each triangle $\tau \in \mathcal{M}_1 \subset \mathcal{T}_1$, we mark the base, and the triangle is bisected to two new children triangles by connecting the peak to the midpoint of the base for reducing the error, and connect the midpoint of the base to the midpoint of the marked edges for the conformity (Fig.4). After all the triangles of subset $\mathcal{M}_1$ are refined, there need more bisections to eliminate the hanging nodes for conformity in general. Our strategy is that for each triangle $\tau \in \mathcal{T}_1 \backslash \mathcal{M}_1$, we divide it as above if there has a hanging node on the base; otherwise we mark the base if and only if the two shortest edges of τ are marked, and then divide the triangle to four new children triangles by connecting the peak and the midpoints of the two shortest edges to the midpoint of the base for conformity respectively; if there is only one hanging node which not on the base, we consider the triangle τ with the hanging node as a quadrilateral and need not completion. For example, in Fig.5(a)(b), we treat the triangle $p(1)p(2)p(3)$ with the hanging node $p(4)$ as a quadrilateral; and in Fig.5(c) we mark the base $\overline{p(2)p(3)}$ since the two shortest edges $\overline{p(1)p(2)}$ and $\overline{p(1)p(3)}$ being marked. We mention that in Fig.3 the dashed line shows the control volume V_P of the hanging node P, and the contribution of quadrilateral $P_4P_1P_2P$ is $\triangle Q_1M_2M_4$, which is different from Fig.2.

After the first loop of AFVM, there should generate quadrilateral elements (a triangular element with a hanging node) in mesh $\mathcal{T}_k$ ($k \geq 2$). Therefore, we need to refine triangular and quadrilateral elements for reducing the error and ensuring

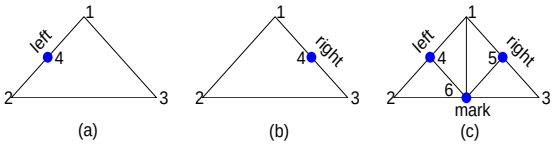

FIGURE 5. Divide a triangle $p(1)p(2)p(3)$ for the conformity that allow hanging node.

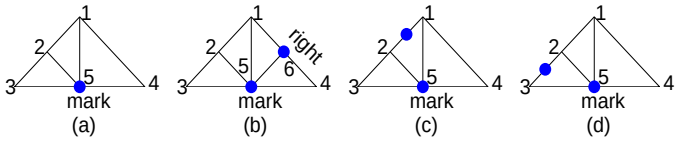

FIGURE 6. Divide a quadrilateral $p(1)p(2)p(3)p(4)$ for reducing the error.

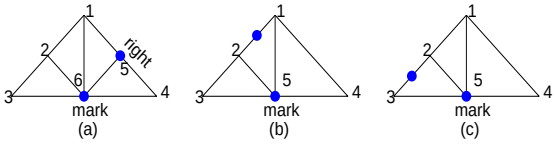

FIGURE 7. Divide a quadrilateral $p(1)p(2)p(3)p(4)$ for the conformity that allow hanging node.

the conformity in the *Refine* step. The unique difference is how to divide a quadrilateral element compare to the first loop. Now, we proceed to present it. The concepts of *base* and *peak* of a quadrilateral are similar to a triangle, for example in Fig.6, vertex $p(1)$ and edge $\overline{p(3)p(4)}$ are the peak and base to the quadrilateral $p(1)p(2)p(3)p(4)$. For each quadrilateral $\tau \in \mathcal{M}_k \subset \mathcal{T}_k$ $(k \geq 2)$, we mark the base, and the quadrilateral is divided to three new children triangles by connecting the peak and hanging node to the midpoint of the base for reducing the error (Fig.6(a)); for conformity we connect the midpoint $p(5)$ of the base to the midpoint $p(6)$ if the edge $\overline{p(1)p(4)}$ is marked (Fig.6(b)), and treat the hanging node as a new vertex if $\overline{p(1)p(2)}$ or $\overline{p(2)p(3)}$ is marked (Fig.6(c)(d)) and need not completion. For each quadrilateral $\tau \in \mathcal{T}_k \backslash \mathcal{M}_k$ $(k \geq 2)$, in order to ensure the conformity, we mark the base as long as one edge of τ is marked, and connect the hanging node $p(2)$ to the midpoint of the base $\overline{p(3)p(4)}$ (Fig.7); we connect the midpoint of the edge $\overline{p(1)p(4)}$ to the midpoint of the base $\overline{p(3)p(4)}$ if $\overline{p(1)p(4)}$ is marked (Fig.7(a)), and treat the hanging node of $\overline{p(1)p(2)}$ or $\overline{p(2)p(3)}$ as a new vertex if it is marked (Fig.7(b)(c)) and need not completion. Then, the subroutine

$$\mathcal{T}_{k+1} = \mathit{Refine}(\mathcal{M}_k, \mathcal{T}_k)$$

outputs hybrid triangular and quadrilateral mesh $\mathcal{T}_{k+1}$ which allow hanging nodes.

In short, the novelty of our AFVM is that we do not have the traditional "completion" procedure in the *Refine* step. To ensure the conformity, a triangular element with a hanging node is treated as a quadrilateral element.

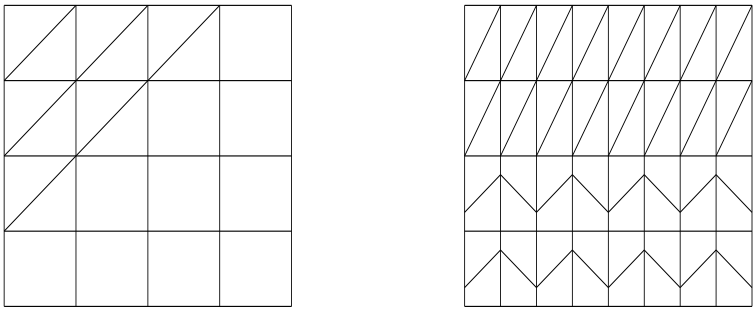

(a) hybrid triangular and rectangular (b) hybrid triangular and trapezoidal

FIGURE 8. Two kinds of hybrid meshes for Example 4.1.

To illustrate the practicability and effectiveness of our AFVM, we are interested in the following type result

$$|u - u_k|_1 \lesssim N_k^{-1/2} \text{ and } \|u - u_k\|_0 \lesssim N_k^{-1}.$$

The numerical results in the next section show that the optimal convergence rate with the above norms can be obtained, even if the exact solution u has lower regularity and with the Ω non convex.

4. Numerical Results

In this section, we present example 4.1 to validate our above theoretical results of FVM, examples 4.2 and 4.3 to the AFVM.

Example 4.1. We consider the problem (1), (2) with $\Omega = [0,1]^2$ and $\alpha = 1$. We choose the exact solution as

$$u(x,y) = \sin(\pi x)\sin(\pi y).$$

Two kinds of hybrid triangular and quadrilateral meshes are implemented. The first kind of meshes are hybrid triangular and rectangular (Fig.8(a)), the second kind of meshes are hybrid triangular and trapezoidal (Fig.8(b)). The numerical results are presented in Table 1 and Table 2. In these two tables, the first column N indicates the number of elements along the x-direction. For example, in Fig.8(a) $N = 4$, and in Fig.8(b) $N = 8$. We see that the optimal accuracy order can be obtained under L^2 and H^1 norms which are consistent with our theoretical results. Furthermore, we also give the accuracy order under L^∞ and $W^{1,\infty}$ norms. We mention that the second kind of meshes are not quasi uniform, since the distance vector of the diagonal midpoints of the trapezoids are $\mathcal{O}(h)$, not $\mathcal{O}(h^2)$.

Example 4.2. We consider the elliptic equation

$$-\nabla \cdot (\alpha \nabla u) = f$$

on the domain $\Omega = \{-1 \le x \le 1, -1 \le y \le 1\}$. We choose $\alpha = 1$ and the exact solution as

$$u(x,y) = e^{-(x^2+y^2)/0.01}.$$

We note that the boundary condition is inhomogeneous for this equation.

We implement our AFVM to this problem, choose the initial triangulation $\mathcal{T}_1$ as in Fig.9(a), the iteration number $n = 30$ and parameter $\theta = 0.3$. Fig.9(b) shows

TABLE 1. Error and convergence order on hybrid triangular and rectangular meshes.

N	L^2 error	Order	H^1 error	Order	L^∞ error	Order	$W^{1,\infty}$ error	Order
2	1.8e-001	/	1.4e+000	/	3.7e-001	/	1.8e+000	/
4	4.0e-002	2.15	6.6e-001	1.05	9.7e-002	1.92	1.0e+000	0.88
8	1.1e-002	1.91	3.4e-001	0.94	2.9e-002	1.75	5.1e-001	0.97
16	2.7e-003	1.96	1.7e-001	0.97	8.0e-003	1.85	2.6e-001	0.99
32	6.9e-004	1.98	8.8e-002	0.98	2.1e-003	1.91	1.4e-001	0.91
64	1.7e-004	1.99	4.4e-002	0.99	5.5e-004	1.95	7.0e-002	0.97
128	4.3e-005	2.00	2.2e-002	1.00	1.4e-004	1.98	3.5e-002	0.99

TABLE 2. Error and convergence order on hybrid triangular and trapezoidal meshes.

N	L^2 error	Order	H^1 error	Order	L^∞ error	Order	$W^{1,\infty}$ error	Order
4	1.0e-001	/	1.1e+000	/	2.5e-001	/	1.9e+000	/
8	2.8e-002	1.89	5.5e-001	0.94	7.5e-002	1.74	1.0e+000	0.91
16	7.0e-003	1.97	2.8e-001	0.98	2.0e-002	1.94	5.1e-001	0.98
32	1.8e-003	1.99	1.4e-001	1.00	5.0e-003	1.97	2.6e-001	0.99
64	4.4e-004	2.00	7.0e-002	1.00	1.2e-003	2.00	1.3e-001	1.00
128	1.1e-004	2.00	3.5e-002	1.00	3.1e-004	2.00	6.4e-002	1.00

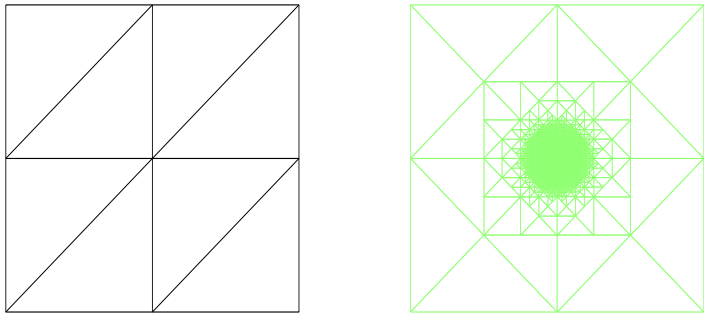

(a) original mesh (b) mesh after 30 iterations

FIGURE 9. Original and adaptive meshes for Example 4.2.

the adaptive mesh after 30 iterative steps. In Fig.10(a), the horizontal coordinate indicate the quantity $\log N_k$, while the vertical coordinate present the logarithm of errors; we depict $\log \|u - u_k\|_{0,\mathcal{T}_k}$ by the solid curve with '$\circ$', $\log \|u - u_k\|_{\infty,\mathcal{T}_k}$ by the solid curve with '$*$', and $-\log N_k$ by the solid curve with '$\square$'. In Fig.10(b), the horizontal coordinate indicate the quantity $\log \sqrt{N_k}$; we depict $\log |u - u_k|_{1,\mathcal{T}_k}$ by the colid curve with '$\circ$', and $-\log \sqrt{N_k}$ by the solid curve with '$\square$'. We observe that $\|u - u_k\|_{0,\mathcal{T}_k}$ and $\|u - u_k\|_{\infty,\mathcal{T}_k}$ decay with N_k^{-1}, and $|u - u_k|_{1,\mathcal{T}_k}$ decay with $N_k^{-0.5}$. Therefore, the optimal convergence order of L^2, H^1 and L^∞ norms can be obtained by using our AFVM. Moreover, the numerical results show that the *Solve* step is stable even if $\mathcal{T}_k$ is not shape regular, since there is an angle equal to π for the quadrilateral element (a triangular element with a hanging node).

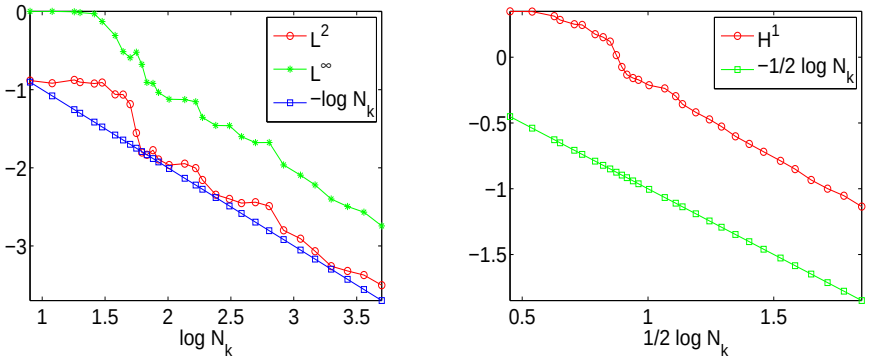

(a) L^2 and L^∞ errors (b) H^1 error

FIGURE 10. The L^2, L^∞ and H^1 errors of our AFVM for Example 4.2.

TABLE 3. The number of elements of each iteration for Example 4.2.

S	N		S	N		S	N	
	NAFVM	SAFVM		NAFVM	SAFVM		NAFVM	SAFVM
1	8	8	11	62	72	21	384	846
2	12	12	12	68	119	22	496	1100
3	18	18	13	76	184	23	638	434
4	20	26	14	84	200	24	830	1854
5	26	34	15	102	234	25	1130	2478
6	30	42	16	136	274	26	1476	3350
7	38	48	17	166	342	27	1982	4552
8	44	54	18	188	412	28	2676	6186
9	50	60	19	240	500	29	3610	8488
10	56	66	20	308	656	30	4996	11650

To illustrate the advantage of our AFVM compare to the standard AFVM need traditional "completion" procedure. We also implement the standard AFVM to example 4.2, the choice of the parameters of these two AFVMs are same in each iteration, and the unique difference is that the standard AFVM needs "completion" procedure compare to our AFVM. We list the number of elements in each iteration of the two AFVMs in Table 3. In this table, S indicates the iterative steps, N indicates the number of elements in each iteration. The NAFVM indicates our novel AFVM, and SAFVM indicates the standard AFVM. It shows that our AFVM decrease the steps of bisection for the conformity compare to the standard AFVM.

Example 4.3. We consider the elliptic equation on the L-shape domain $\Omega = \{-1 \leq x \leq 1, -1 \leq y \leq 1\} \backslash \{0 \leq x \leq 1, -1 \leq y \leq 0\}$ with $\alpha = 1$ and the exact solution as

$$u(x, y) = r^{\frac{2}{3}} \sin(\frac{2\theta}{3}),$$

where $r = (x^2 + y^2)^{\frac{1}{2}}$ and $\theta = \arctan \frac{y}{x}$. A direct calculation yields the right-hand side function $f = 0$. We note that the domain Ω is not convex and the boundary condition is inhomogeneous for this equation.

We implement our AFVM to this problem, choose the initial triangulation $\mathcal{T}_1$ as in Fig.11(a), the iteration number $n = 30$ and parameter $\theta = 0.3$. Fig.11(b)

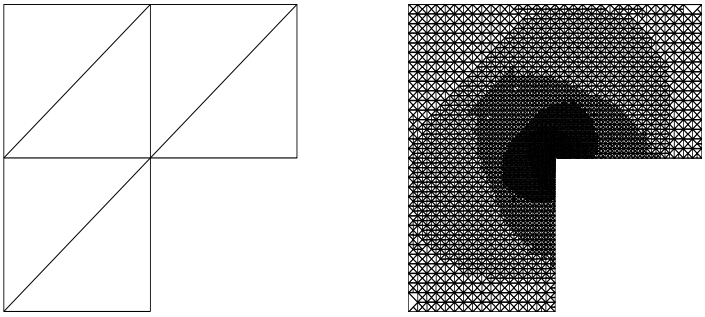

(a) original mesh (b) mesh after 30 iterations

FIGURE 11. Original and adaptive meshes for Example 4.3.

TABLE 4. Error and convergence order of our AFVM for Example 4.3.

S	N_k	L^2 error	Order	H^1 error	Order	L^∞ error	Order
26	2342	2.6e-004	1.82	2.4e-002	1.01	8.6e-004	1.23
27	3138	2.2e-004	1.14	2.1e-002	0.97	6.6e-004	1.78
28	4196	1.5e-004	2.81	1.8e-002	1.02	5.5e-004	1.33
29	5672	1.1e-004	2.14	1.6e-002	0.98	4.2e-004	1.81
30	7674	7.8e-005	2.16	1.3e-002	1.00	3.5e-004	1.22

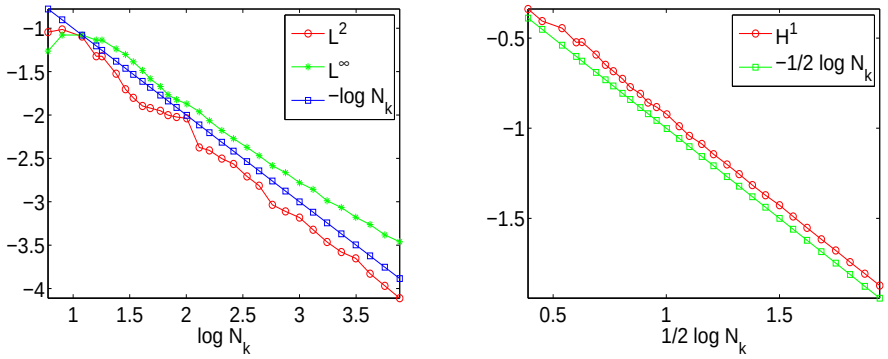

(a) L^2 and L^∞ errors (b) H^1 error

FIGURE 12. The L^2, L^∞ and H^1 errors of our AFVM for Example 4.3.

shows the adaptive mesh after 30 iterative steps. The partial numerical results are presented in Table 4. Fig.12 shows the complete results of the true error with respect to N_k. We observe that $\|u-u_k\|_{0,\mathcal{T}_k}$ and $|u-u_k|_{1,\mathcal{T}_k}$ decay with N_k^{-1} and $N_k^{-0.5}$ respectively. Note that for linear FVM on triangle or bilinear FVM on quadrilateral, the convergence rate for $\|u-u_h\|_0$ and $|u-u_h|_1$ are $\mathcal{O}(h^2) \sim \mathcal{O}(N^{-1})$ and $\mathcal{O}(h) \sim \mathcal{O}(N^{-0.5})$ for uniform meshes, if u is sufficiently regular. In our numerical example, $u \in H^{1+\frac{2}{3}-\varepsilon}(\Omega)$ for all $\varepsilon > 0$ and $u \notin H^2(\Omega)$, and the domain Ω is not convex, we could not obtain these results if we use uniform meshes. However, the optimal convergence order of L^2 and H^1 norms can be obtained by using our

TABLE 5. The number of elements of each iteration for Example 4.3.

S	N		S	N		S	N	
	NAFVM	SAFVM		NAFVM	SAFVM		NAFVM	SAFVM
1	6	6	11	59	59	21	76	672
2	8	8	12	69	75	22	752	886
3	12	12	13	82	92	23	1001	1182
4	16	16	14	101	112	24	1320	1564
5	18	18	15	130	142	25	1750	2100
6	24	24	16	160	190	26	2342	2816
7	29	29	17	206	242	27	138	3778
8	34	34	18	261	302	28	4196	5084
9	41	41	19	344	393	29	5672	6836
10	48	49	20	440	506	30	7674	9274

AFVM. From Table 4 and Fig. 12(a), we also observe that the convergence order of $\|u-u_k\|_{\infty,\mathcal{T}_k}$ is bigger than 1. We also implement the standard AFVM to example 4.3, and the results are listed in Table 5.

Acknowledgments

The work was supported in part by the following Grants: the special project High performance computing of National Key Research and Development Program 2016YFB0200604, NSFC 11571384, Guangdong Provincial NSF 2014A030313179, the Fundamental Research Funds for the Central Universities 16lgjc80.

References

[1] R. E. Bank and D. J. Rose, Some error estimates for the box method, SIAM J. Numer. Anal., 24(1987) 777-787.
[2] T. Barth and M. Ohlberger, Finite volume Methods: Foundation and Analysis. In: Encyclopedia of Computational Mechanics, vol. 1, chapter 15, Wiley 2004.
[3] P. Binev, W. Dahmen and R. DeVore, Adaptive finite element methods with convergence rates, Numer. Math., 97(2004) 219-268.
[4] D. Braess, Finite Elements: Theory, Fast Solvers, and Applications in Solid Mechanics, 3rd ed, Cambridge University Press 2007.
[5] Z. Cai, On the finite volume element method, Numer. Math., 58(1991) 713-735.
[6] C. Carstensen, R. Lazarov, S. Tomov, Explicit and averaging a posteriori error estimates for adaptive finite volume methods, SIAM J. Numer. Anal., 42(2005) 2496-2521.
[7] L. Chen, Short bisection implementation in matlab, Research note 2006.
[8] Y. Chen, Y. Li, Z. Sheng and G. Yuan, Adaptive bilinear element finite volume methods for second-order elliptic problems on nonmatching grids, J. Sci. Comput., 64(2015) 130-150.
[9] P. G. Ciarlet, The Finite Element Method for Elliptic Problems, North-Holland, Amsterdam 1978.
[10] W. Dörfler, A convergent adaptive algorithm for Poisson's equation, SIAM J. Numer. Anal., 33(1996) 1106-1124.
[11] C. Erath and D. Praetorius, A posteriori error estimate and adaptive mesh refinement for the cell-centered finite volume method for elliptic boundary value problems, SIAM J. Numer. Anal., 47(2008) 109-135.
[12] C. Erath and D. Praetorius, Adaptive vertex-centered finite volume methods with convergence rates, SIAM J. Numer. Anal., 54(2016) 2228-2255.
[13] R. E. Ewing, T. Lin and Y. Lin, On the accuracy of the finite volume element method based on piecewise linear polynomials, SIAM J. Numer. Anal., 39(2002) 1865-1888.
[14] Z. Lai, B. Wu and Q. Zou, Finite volume method on hybrid meshes for coastal ocean model, Int. J. Numer. Anal. Mod., 13(2016) 310-317.
[15] R. Lazarov, I. Michev and P. Vassilevski, Finite volume methods for convection-diffusion problems, SIAM J. Numer. Anal., 33(1996) 31-55.

[16] R. J. LeVeque, Finite Volume Methods for Hyperbolic Problems, Cambridge Texts in Applied Mathematics, Cambridge University Press, Cambridge 2002.
[17] R. Li, Z. Chen and W. Wu, The Generalized Difference Methods for Partial Differential Equations: Numerical Analysis of Finite Volume Methods, Marcel Dikker, New York 2000.
[18] Y. Li and R. Li, Generalized difference methods on arbitrary quadrilateral networks, J. Comput. Math., 17(1999) 653-672.
[19] T. Lin and X. Ye, A posteriori error estimates for finite volume method based on bilinear trial functions for the elliptic equation, J. Comput. Appl. Math., 254(2013) 185-191.
[20] Y. Lin, M. Yang and Q. Zou, L^2 error estimates for a class of any order finite volume schemes over quadrilateral meshes, SIAM J. Numer. Anal., 53(2015) 2030-2050.
[21] J. Lv and Y. Li, L^2 error estimate of the finite volume element methods on quadrilateral meshes, Adv. Comput. Math., 33(2010) 129-148.
[22] R. H. Macneal, An asymmetrical finite difference network, Quart. Appl. Math., 11(1953) 295-310.
[23] S. Nicaise, A posteriori error estimations of some cell-centered finite volume methods, SIAM J. Numer. Anal., 43(2005) 1481-1503.
[24] C. Ollivier-Gooch and M. Altena, A high-order-accurate unconstructed mesh finite-volume scheme for the advection-diffusion equation, J. Comput. Phys., 181(2002) 729-752.
[25] T. Schmidt, Box schemes on quadrilateral meshes, Computing, 51(1993) 271-292.
[26] C.-W. Shu, High-order finite difference and finite volume weno schemes and discontinuous galerkin methods for cfd, J. Comput. Fluid Dyn. 17(2003) 107-118.
[27] M. Vohralík, Residual flux-based a posteriori error estimates for finite volume and related locally conservative methods, Numer. Math., 111(2008) 121-158.
[28] X. Wang and Y. Li, L^2 error estimates for high order finite volume methods on triangular meshes, SIAM J. Numer. Anal., 54(2016) 2729-2749.
[29] J. Xu and Q. Zou, Analysis of linear and quadratic simplicial finite volume methods for elliptic equations, Numer. Math., 111(2009) 469-492.
[30] J. Xu, Y. Zhu and Q. Zou, New adaptive finite volume methods and convergence analysis, Preprint, Pennsylvania State University 2006.
[31] Z. Zhang and Q. Zou, Some recent advances on vertex centered finite volume element methods for elliptic equations, Sci. China Mathematics, 56(2013) 2507-2522.
[32] Z. Zhang and Q. Zou, A family of finite volume schemes of arbitrary order on rectangular meshes, J. Sci. Comput., 58(2014) 308-330.
[33] Z. Zhang and Q. Zou, Vertex-centered finite volume schemes of any order over quadrilateral meshes for elliptic boundary value problems, Numer. Math., 130(2015) 363-393.
[34] O. C. Zienkiewicz and J. Zhu, The superconvergent patch recovery and a posteriori error estimates. Part 1: The recovery technique, Int. J. Numer. Meth. Eng., 33(1992) 1331-1364.
[35] O. C. Zienkiewicz and J. Zhu, The superconvergent patch recovery and a posteriori error estimates. Part 2: Error estimates and adaptivity, Int. J. Numer. Meth. Eng., 33(1992) 1365-1382.
[36] Q. Zou, Hierarchical error estimates for finite volume approximation solution of elliptic equations, Appl. Numer. Math., 60(2010) 142-153.
[37] Q. Zou, An unconditionally stable quadratic finite volume scheme over triangular meshes for elliptic equations, J. Sci. Comput., 70(2017) 112-124.

School of Mathematics, Sun Yat-sen University, Guangzhou, 510275, China
E-mail: zhouyh9@mail2.sysu.edu.cn

Corresponding author. School of Data and Computer Science and Guangdong Province Key Laboratory of Computational Science, Sun Yat-sen University, Guangzhou, 510275, China
E-mail: mcszqs@mail.sysu.edu.cn